Astron. Astrophys. 343, 519–530 (1999)

ASTRONOMY
AND
ASTROPHYSICS

Barium abundances in cool dwarf stars as a constraint to s- and r-process nucleosynthesis⋆

L. Mashonkina[1], **T. Gehren**[2], **and I. Bikmaev**[1]

[1] Department of Astronomy, Kazan State University, Kremlevskaya 18, Kazan 8, 420008, Russia
[2] Institut für Astronomie und Astrophysik der Universität München, Scheinerstrasse 1, D-81679 München, Germany

Received 11 September 1998 / Accepted 1 December 1998

Abstract. We revise barium abundances in 11 cool stars with metallicities ranging from -2.65 to 0.05. The results are based on differential NLTE model atmosphere analyses of spectra that have a typical S/N of 200 and a resolution of 40000 or 60000. To minimize systematic errors of theoretical modeling and to be sure that elemental surface abundances are not contaminated by thermonuclear reaction products from the stellar interior the sample is confined to main-sequence and turnoff stars with only two subgiants added. Stellar fundamental parameters are derived from either (V-K) colours or Balmer line profiles for the effective temperature, from HIPPARCOS parallaxes for the surface gravity and from the LTE analyses of the Fe II line profiles for metal abundance and microturbulence values. The statistical equilibrium of Ba II is investigated with a model atom containing 41 levels of Ba II plus the ground state of Ba III. NLTE effects depend on the metallicity of a star: they increase the equivalent widths compared with LTE for [Fe/H] > -2, and they show the opposite behaviour at lower metallicities. Empirical evidence for the necessity to include H atom collisions in the statistical equilibrium of Ba II is found from comparison of Ba abundances in the metal-poor stars derived from the different spectral lines. The formula of Drawin with a scaling factor of 1/3 gives quite sufficient results. [Ba/Fe] abundance ratios are approximately solar above [Fe/H] ~ -2.2 where they decrease rapidly by 0.5–0.6 dex. The direct method based on the hyperfine structure (HFS) of the resonance line of the odd isotopes is suggested to estimate the contribution of the s- and r- process to Ba synthesis. Its application requires the knowledge of the total Ba abundance that can be deduced from the subordinate lines free of HFS. Thus, we cannot estimate the ratio of the s- and r-processes for the two most metal-deficient stars of our sample. Our conclusion is that the s-process dominated Ba production, at least, for the metal-poor stars with [Fe/H] > -2.2.

Key words: line: formation – nuclear reactions, nucleosynthesis, abundances – stars: abundances – stars: fundamental parameters – stars: late-type

Send offprint requests to: L. Mashonkina (ml@astro.ksu.ras.ru)

⋆ Based on observations at the German Spanish Astronomical Center, Calar Alto, Spain

1. Introduction

Barium is one of the most abundant and best observable chemical elements produced in neutron capture reactions. It is displayed in spectra of F-G stars with several spectral lines of two Ba II multiplets: $\lambda\lambda$455.4, 493.4 nm ($6s^2\mathrm{S} - 6p^2\mathrm{P}^\circ$) and $\lambda\lambda$585.3, 614.1, 649.6 nm ($5d^2\mathrm{D} - 6p^2\mathrm{P}^\circ$). Three of these lines are nearly free of blends. As Ba II is the dominant ionization stage in such atmospheres and the observable lines arise from the ground state ($6s$) or the low-excited $5d$ term (with an excitation energy of ~ 0.7 eV) these Ba II lines can be detected even in extremely metal-poor stars.

Two types of neutron capture reactions are generally distinguished: the s-process (slow) and the r-process (rapid) depending on the amount of the neutron flux available. According to Cameron (1982) the even Ba isotopes are mostly synthesized in the s-process whereas the odd isotopes are produced in both processes. In the solar system matter the r-process dominates $^{135}\mathrm{Ba}$ (r: s = 25: 10), and it contributes approximately one third to $^{137}\mathrm{Ba}$ (r: s = 38: 100). In total the ratio of the r-process to the s-process Ba atoms is approximately 12: 88. The most recent study (Burris et al. 1998) of the solar system r/s mixture gives a value close to 15: 85. Therefore one concludes that the contribution of the s-process to Ba production integrated from the beginning of the Universe to the birth of the solar system is greater than the contribution of the r-process. But the relative contributions of these processes might vary with time. The run of barium to iron abundances [Ba/Fe] is often used to constrain Galactic nucleosynthesis and to provide the information about the relative importance of the s- and r-processes in various epochs.

Ba abundances in cool stars were determined by a number of authors beginning with the pioneering study of Spite & Spite (1979). Mathews et al. (1992) have superposed the data from 14 different studies on a [Ba/Fe]–[Fe/H] diagram to compare them with the predictions of theoretical models. From inspection of those data two features can be seen. Firstly, the trend of [Ba/Fe] with [Fe/H] at [Fe/H] < -1.5. For the extremely metal-poor stars ([Fe/H] < -2.5) barium is underabundant relative to iron by 1–1.5 dex, and [Ba/Fe] grows with increasing metallicity and reaches a solar value at about [Fe/H]$= -1.5$.

The second feature is the large scatter of the data. It is within 0.5 dex at [Fe/H] > -1.5 and increases up to 1 dex for more metal-poor stars. A similar trend and even larger scatter of the data up to 1.5–2 dex can be noted in Fig. 5 of Ryan et al. (1990) who compiled the results of 6 analyses. In both compilations the systematic differences from author-to-author are evident. For example, [Ba/Fe] of Leep & Wallerstein (1981) or Gilroy et al. (1988) is lower on average by 0.5 dex than the results of Magain (1989) or Peterson et al. (1990). Such discrepancies are probably arising from the use of giants and supergiants in most of the studies due to the fact that Ba II lines are more easily measured in spectra of luminous stars than in dwarfs. But two points should be carefully considered whenever giants and supergiants are involved. Firstly, theoretical modeling meets many unsolved problems: atmospheric extension effects, velocity fields, opacity, and, therefore uncertainties of stellar parameters and elemental abundances should be expected. The second point: can we be sure that atmospheric abundances have not been contaminated by nuclear reaction products synthesized during the star's evolution? Samples of cool stars with $\log g > 3$ were analyzed by Magain (1989), Edvardsson et al. (1993) and Bikmaev et al. (1996). Inspection of their results suggests that there is no trend of [Ba/Fe] with metallicity at [Fe/H] > -2 though the scatter of individual data is rather large and may reach 0.5 dex. At lower metallicities only the data of Magain (1989) are available, and they display an increasing Ba underabundance with decreasing [Fe/H].

In this paper we intend to improve barium abundances in cool stars. Only main sequence (MS) or close to MS stars are selected to be sure that atmospheric abundances reflect the real chemical composition of interstellar matter out of which the star was formed and to reduce methodical errors connected with the determination of fundamental parameters and modeling of stellar atmospheres. Our sample includes 8 dwarfs with effective temperatures $T_{\rm eff}$ from 5110 K to 6060 K, surface gravities $\log g$ from 4.18 to 4.60 and metallicities [Fe/H] from 0.05 down to -2.60 plus two G-type metal-poor subgiants. Procyon is added as a reference star with its fundamental parameters well known from direct methods. Ba and Fe abundances are determined differentially with respect to the Sun which means that oscillator strengths f_{ij} and van der Waals damping constants C_6 were determined in advance from solar line profile fitting where Procyon served as a second comparison star.

Compared with previous studies our techniques of Ba abundance determination have advanced in three points. Firstly, based on the high-resolution spectra elemental abundances and microturbulence values $V_{\rm mic}$ are derived from line profile fitting and not from equivalent widths W_λ. Since even at $R = 60000$ Ba line profiles are not resolved, the significance of this fitting process is limited to a coarse consistency test including an elaborate determination of both large-scale velocity fields (macroturbulence and rotation) and an instrumental profile. A short description of observations is given in Sect. 2. Secondly, better methods have been used to determine stellar parameters: $T_{\rm eff}$ is still mostly from (V-K) colours with a few determinations from Balmer lines, $\log g$ is based on HIPPARCOS data, [Fe/H] and $V_{\rm mic}$ are from Fe II lines. The procedure of their derivation is described in Sect. 3. And finally, non-local thermodynamical equilibrium (NLTE) line formation is considered to obtain theoretical Ba II line profiles. The method of NLTE calculations for Ba II is described in Sect. 4. In Sect. 5 we discuss the results, NLTE effects in Ba II line formation of cool stars, solar Ba II line profile fitting and the run of [Ba/Fe] with [Fe/H]. In addition, we present the direct method for an estimate of the s- and r- process contributions to Ba synthesis. Our method takes advantage of the hyperfine structure (HFS) affecting the Ba II resonance line of the odd isotopes. The odd-to-even isotope ratio can be derived from a comparison of the observed λ455.4 nm line intensity with the theoretical one corresponding to different isotopic ratios provided that the total Ba abundance is deduced from the subordinate lines that are free of HFS effects. This ratio is a measure of the r- to s-process relation. Our method of estimating the r/s mixture of a star was also proposed by Cowley & Frey (1989) who pointed out the importance of accounting for HFS in Ba abundance determinations. Magain & Zhao (1993) and Magain (1995) have suggested a different method based on measuring the broadening of the Ba II λ 455.4nm line, and they have applied it to the extremely metal-poor star HD 140283. In this study we will increase the total number of stars with r/s mixture estimated.

2. Observations

Our results are based on spectra observed by K. Fuhrmann and M. Pfeiffer using the fiber optics cassegrain échelle spectrograph FOCES fed by the 2.2m telescope at the Calar Alto observatory during two observing runs in September 1995 and in May 1997. The 1995 spectra were exposed to a 1024×1024 $24\,\mu$ CCD, and the resolving power was ~ 40000. In May 1997 a 2048×2048 $15\,\mu$ CCD was employed at $\lambda/\Delta\lambda \sim$60000. Almost all the stars were observed at least twice with the real signal-to-noise ratio of about 200 (Fuhrmann 1998). Details with respect to the FOCES spectrograph and the data reduction can be found in Pfeiffer et al. (1998). Table 1 lists the stars selected.

The data reduction for most of the stars has been performed according to the description given in Pfeiffer et al. (1998). Only small corrections to continuum rectification and wavelength shifts were necessary to obtain the final spectra. The instrumental profile is found from comparison of the FOCES Moon spectrum with the Kitt Peak Solar Flux Atlas (Kurucz et al. 1984). A Gaussian of $4.6 \pm 0.2\,{\rm km\,s^{-1}}$ provides the best fit to the September 1995 spectra (Fuhrmann et al. 1997a), and $3.2 \pm 0.2\,{\rm km\,s^{-1}}$ is appropriate for the May 1997 observations (Fuhrmann 1998).

3. Model atmospheres and stellar parameters

3.1. Model atmospheres

Our analyses are all based on the same type of model, irrespective of temperature, gravity or metal abundance. We used line-blanketed LTE model atmospheres recently generated and

Table 1. Stellar parameters of the selected sample. Most of the entries are self-explanatory; π''_{HIP} denotes the Hipparcos parallax. $T_{\rm eff}$ preceded by an asterisk refers to spectroscopic determination (see Sect. 3.2)

HD/BD	$T_{\rm eff}$ [K]	$\log g$	[Fe/H]	$V_{\rm mic}$ [km s^{-1}]	Mass [$M_\odot$]	$\pi''_{\rm HIP}$ [10^{-3}]
[1]6582	*5390	4.52	−0.83	0.9	0.75	132.40
19445	5930	4.22	−1.97	1.3	0.74	25.85
45282	*5280	3.24	−1.50	1.4	0.82	7.34
[2]61421	6500	4.04	0.00	1.9		
[3]103095	*5110	4.67	−1.36	0.9	0.64	109.21
140283	5640	3.65	−2.30	1.5	0.80	17.44
[4]186408	5890	4.22	0.05	1.0	0.93	46.25
194598	5900	4.29	−1.21	1.4	0.83	17.94
201891	5900	4.30	−1.05	1.2	0.83	28.26
[5]3°740	6060	4.18	−2.60	2.0	0.80	7.80
[6]66°268	*5340	4.60	−2.20	0.9	0.63	17.58

[1] HR 321 = μ Cas, [2] HR 2943 = Procyon, [3] HR 4550 = Groombridge 1830, [4] HR 7503 = 16 Cyg A, [5] G84-29, [6] G246-38

discussed by Fuhrmann et al. (1997a). Three aspects are worth mentioning:

1. The opacity distribution functions (ODF) have been interpolated from Kurucz' (1994) ODF tables for the proper stellar metallicities. In addition, they were scaled by -0.16 dex to put the iron opacity calculated by Kurucz with $\log \varepsilon_{\rm Fe} = 7.67$ into correspondence with the improved meteoritic value $\log \varepsilon_{\rm Fe} = 7.51$ which we believe to be the most probable representation of the solar mixture. We refer to abundances on the usual scale where $\log \varepsilon_{\rm H} = 12$.
2. The b-f opacities were computed with solar abundances from Holweger (1979) scaled by the stellar metallicity. In addition, at [Fe/H] < -0.6 opacities due to α-elements (O, Ne, Mg, Si, S, Ar, Ca and Ti) were calculated with elemental abundances increased by 0.4 dex to take into account the observed enhancement of these elements in metal-poor stars.
3. The mixing-length parameter l/H_p was adopted to be 0.5.

3.2. Stellar parameters

Only for Procyon the stellar parameters $T_{\rm eff}$ and $\log g$ are known from direct methods. As Procyon is a close-by visual binary the direct measurements of integrated flux and angular diameter supply a precise value for $T_{\rm eff}$, and accurate values for stellar mass and consequently, surface gravity can be derived. From a detailed discussion of its parameters in Fuhrmann et al. (1997a) we suggest the best values: $T_{\rm eff} = 6500$ K and $\log g = 4.04$. The Fe abundance [Fe/H] = 0 and $V_{\rm mic}$ are taken from Fuhrmann (1998) who derived them from the Fe II line profile fitting.

For 6 of the other stars $T_{\rm eff}$ was estimated by Bikmaev et al. (1996) from (V-K) or (R-I) colour indices using their own calibration colour index – $T_{\rm eff}$ based on the infrared flux method. For remaining 4 stars which are absent in the list of Bikmaev et al. (1996) $T_{\rm eff}$ was obtained from Balmer line profile fitting by Fuhrmann (1998: HD6582, HD45282, HD103095) and Grupp (1997: G246-38) and they have been kindly put at our disposal in advance of publication. They are indicated by asterisks in Table 1. We realize that the use of different $T_{\rm eff}$ scales can result in systematic errors in element abundances between different stars, and we have estimated such an error for HD194598. Four stars of our sample with photometric $T_{\rm eff}$ are common with the selection of Fuhrmann (1998) who evaluates $T_{\rm eff}$ from Balmer line profile fitting. For three stars the difference between photometric and spectroscopic temperatures is less than 100 K, and for HD194598 it is 158 K. For the stellar parameters derived by Fuhrmann (1998) $T_{\rm eff}$ = 6058 K, $\log g$ = 4.27, [Fe/H] = −1.12 we found [Ba/H] = −1.02, and therefore [Ba/Fe] = 0.10. We show below that the same value of [Ba/Fe] is derived with the stellar parameters adopted in this paper. So, a possible error of $T_{\rm eff}$ of about 150 K does not very much affect relative abundances [Ba II/Fe II].

Accurate surface gravities are especially important for our study because the spectral lines of the dominant ionization stage are used to determine Ba abundances (Ba II lines) and metallicity (Fe II lines). The well-known relation between g, stellar mass M, radius R and $T_{\rm eff}$ is used to estimate g, where square brackets denote the logarithmic ratio with respect to the solar value:

$$[g] = [M] + 4[T_{\rm eff}] + 0.4({\rm M_{bol}} - {\rm M_{bol\odot}}) \quad . \qquad (1)$$

The absolute bolometric magnitudes $\rm M_{bol}$ are obtained using the HIPPARCOS parallaxes (ESA 1997) and the bolometric corrections BC from VandenBerg (1992). For the Sun the absolute visual magnitude ${\rm M_{V\odot}} = 4.83$ and ${\rm BC_\odot} = -0.12$ (Allen 1973) are adopted. For the metal-poor stars the mass is estimated from its position in the ${\rm M_{bol}} - \log T_{\rm eff}$ diagram interpolating in the set of oxygen-enhanced isochrones of 12 Gyr–16 Gyr constructed by Bergbusch & VandenBerg (1992). Changing the age by 4 Gyr implies mass changes of less than 10%. Following Nissen et al. (1997) we shifted the isochrones by a constant in $\log T_{\rm eff}$ in order to get the best possible fit between the unevolved stars and the corresponding part of the isochrones. That displacement consists of -0.022 for stars with [Fe/H] < -1.4 and -0.012 for $-1.4 <$ [Fe/H] < -0.8. For HD186408 we used the evolutionary tracks for solar metallicity given in Fuhrmann et al. (1997b). The error of the gravity depends on the parallax error which does not exceed 13% for our selection of stars, on the stellar mass error which is within 10% and on $T_{\rm eff}$ error which is believed no more than 100 K. In total, these errors correspond to an error of $\log g$ of less than 0.1.

The Fe II lines are believed insensitive (or only slightly sensitive) to NLTE effects, and we prefer to estimate [Fe/H] and $V_{\rm mic}$ from the Fe II line profile fitting. The oscillator strengths of some selected Fe II lines have been improved from the analysis of corresponding profiles in the Kitt Peak Solar Flux Atlas (Kurucz et al. 1984). We estimate our iron abundance determinations to be better than 0.1 dex and our values of $V_{\rm mic}$ are erroneous by no more than 0.1 km s^{-1}. All the parameters are given in Table 1.

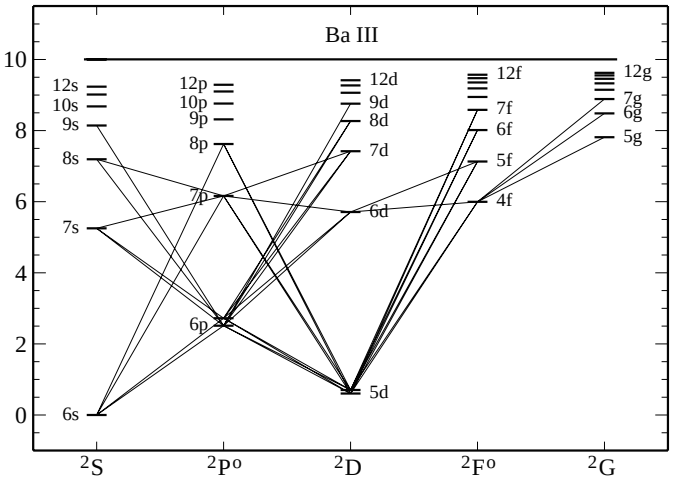

Fig. 1. The Ba II model atom. The linearized transitions are shown as solid lines

4. Method of calculations

4.1. Model atom

We have started from the earlier NLTE study of Ba II (Mashonkina & Bikmaev 1996), however, the calculus has been advanced. We describe briefly the new results.

The Ba II model atom now contains all the levels with $n \leq 12$ and $l \leq 4$. The doublet fine structure is neglected except for the $5d^2\mathrm{D}$ and $6p^2\mathrm{P}^\circ$ splitting. Based on the small excitation energy differencees between nf and $(n-1)g$ levels starting from $n = 8$ we combine such pairs of levels into single levels. Thus, 35 bound levels of Ba II and the ground state of Ba III are included into the model atom. The corresponding Grotrian diagram is shown in Fig. 1. The Ba I levels from the ground state up to $n = 9$ are taken into account only for number conservation. In all stellar atmospheres considered the ratio n(BaI)/n(Ba II) is smaller than 10^{-4} due to the low ionization energy of Ba I: χ(Ba I) = 5.2 eV, and no transitions in the BaI atom can change the Ba II level populations.

The energy levels are from Roig & Tondello (1975). The Ba II transition probabilities from Wiese & Martin (1980) and Miles & Wiese (1969) are believed to be the best. If they are absent the data of Kurucz (1994) or Lindgard & Nielsen (1977) are taken giving preference to the first of them. The photoionization cross-sections for the $l \leq 3$ levels have been kindly provided by Hofsaess (1979). The only exception is the Ba II ground state for which the data by Shevelko (1974) are preferred. For the g-levels the hydrogenic cross-sections are computed.

In cool stars the ratio of electrons to hydrogen atoms decides about the importance of either type of inelastic collisions. Drawin's (1968) formula as described by Steenbock & Holweger (1984) is widely used to calculate hydrogenic collisions, and it suggests that their influence is comparable with electron impact. In our calculations we take into account both types of collisions. Electron impact ionization cross-sections are from the measurements of Peart et al. (1973) and Feeney et al. (1972) for the Ba II ground state and from Drawin (1961) for other levels. For electron impact excitation we use the data of Crandall et al. (1974) and Sobelman et al. (1981); if they are absent the formula of van Regemorter (1962) for allowed transitions and Allen (1973) for forbidden ones has been adopted. As for hydrogenic collisions we use the formula of Steenbock & Holweger (1984) for allowed transitions and Takeda (1992) for forbidden ones. Since these formulae provide only an order of magnitude estimate, the cross-sections were multiplied by appropriate scaling factors in order to produce the best fit to the solar Ba II level populations and line profiles.

4.2. Statistical equilibrium calculations

The Ba II statistical equilibrium is calculated using the code NONLTE3 (Sakhibullin 1983) which is based on the complete linearization method as described by Auer & Heasley (1976). The linearization includes 40 radiative line transitions which are treated with Doppler broadening, radiative and van der Waals damping where γ_R is the classical damping constant and C_6 is calculated according to Unsöld (1955). Background opacity includes b-f and f-f transitions of H, H^-, H_2^+ and He I; b-f transitions of neutral atoms and first ions of the most abundant other elements; Rayleigh scattering and electron scattering; quasi-molecular hydrogen absorption according to Doyle (1968), molecular absorption from 11 of the most abundant molecules, and line absorption. The line opacity introduced by both the H I and metal lines is taken into account by explicitly including it in the calculations. The metal line list has been extracted from Kurucz' (1994) compilation and contains about 170000 lines of neutral atoms and the two first ionization stages between 91.2 and 10000 nm.

4.3. Line profile calculations

Three Ba II lines relatively free of blends are used in Ba abundance calculations. Their atomic data are given in Table 2.

Radiative damping constants are computed explicitly: $\gamma_R = \sum_{i<u} A_{ui}$. Here only transitions from the upper level u should be taken into account because the lines arise from the ground state or the metastable one. The quadratic Stark effect estimated for the resonance line with the data from Fleurier et al. (1977) and Platisa et al. (1971) turns out to be neglegible for stars like the Sun, and it is not taken into account in line profile analysis. Van der Waals damping constants C_6 are evaluated from the solar line fits (see Sect. 5.2).

Ba II lines are strongly affected by hyperfine structure (HFS). Barium is represented by five or more isotopes with significant contributions from the odd nuclei: for solar system matter the ratio of the even Ba isotopes to the odd ones n(^{134}Ba +^{136}Ba +^{138}Ba): n(^{135}Ba +^{137}Ba) is 82:18 according to Cameron (1982). Isotopic shifts are very small ($\leq$ 2 mÅ) but the odd isotopes have hyperfine splitting of their levels resulting in several HFS components for each spectral line. The data on HFS of Ba II levels by Brix & Kopfermann (1952) are commonly used. We have reviewed the literature for more recent data. In Table 3 we compare the fine structure constant

Table 2. Atomic data for the Ba II lines. Most of the entries are self-explanatory; f_{ij} of the HFS components correspond to Ba isotopic abundances of solar system matter; we give the classic Unsöld collisional damping constant $\log C_6$ and the correction $\Delta \log C_6$ from solar line profile fitting

λ, [nm]	HFS $\Delta\lambda$ [pm]	HFS f_{ij}	$\log \gamma_R$	$\log C_6$	$\Delta \log C_6$
455.403[a]	0.0	0.597	8.199	−32.11	0.64
	1.80	0.081			
	−3.40	0.0487			
585.370[b]	–	0.0247	8.199	−31.85	1.60
649.690[c]	0.0	0.0862	8.100	−31.89	0.74
	−0.41	0.00357			
	0.89	0.00704			
	−0.37	0.00819			

[a] $6s^2\mathrm{S}_{1/2} - 6p^2\mathrm{P}^\circ_{3/2}$
[b] $5d^2\mathrm{D}_{3/2} - 6p^2\mathrm{P}^\circ_{3/2}$
[c] $5d^2\mathrm{D}_{3/2} - 6p^2\mathrm{P}^\circ_{1/2}$

Table 3. Hyperfine structure constants in units of $10^{-3}\,\mathrm{cm}^{-1}$ from Brix & Kopfermann (1952), A(1952), for the Ba II levels compared with the most recent experimental data A(new)

Term	^{135}Ba A(1952)	^{135}Ba A(new)	^{137}Ba A(1952)	^{137}Ba A(new)
$6s^2\mathrm{S}_{1/2}$	121.5	119.8[b]	135.5	134.0[c]
$5d^2\mathrm{D}_{3/2}$	–	5.7[a]	–	6.4[a]
$5d^2\mathrm{D}_{5/2}$	–	−0.3[a]	–	−0.2[a]
$6p^2\mathrm{P}^\circ_{1/2}$	20.8	–	23.2	25.4[a]
$6p^2\mathrm{P}^\circ_{3/2}$	4.0	3.8[a]	5.0	4.2[a]

[a] Silverans et al. 1980
[b] Becker & Werth 1983
[c] Blatt & Werth 1982

A from the high resolution laser measurements of Silverans et al. (1980), Blatt & Werth (1982) and Becker & Werth (1983) with the data of Brix & Kopfermann (1952). The agreement is satisfactory; the new data change the wavelength separations by no more than 1% for the resonance line and no more than 10% for λ649.6nm. As is evident from Table 3 level splitting is at maximum for the ground state, so that the components of the resonance line $\lambda 455.4$nm are separated by 5.2 pm. In total, $\lambda 455.4$nm has 15 HFS components (Biehl 1976) and, fortunately, the 3-component simplification given by Rutten (1978) is sufficiently precise. We accept it in this paper based on our test computations which show that the theoretical profile with 15 HFS components differs from the 3-component model by no more than 0.017 of the continuum flux. It is very important for our subsequent analysis (Sect. 5.4) that the unshifted component is produced by only the even isotopes and the blue and red components only by the odd isotopes. Their relative intensities depend on Ba isotopic abundances. The oscillator strengths corresponding to the terrestial isotopic ratios are given in Table 2. The total width of the patterns of $\lambda 585.3$ nm is much smaller (1pm) and is neglected. The 2.3 pm wide patterns of the $\lambda 649.6$ nm line are considered as a four component model according to Rutten (1978), too.

The synthetic line profiles are computed using the departure coefficients $b_i = n_i^{\mathrm{NLTE}}/n_i^{\mathrm{LTE}}$ of the Ba II levels from the code NONLTE3 and the LTE assumption for other atoms. Here, n_i^{NLTE} and n_i^{LTE} are the statistical equilibrium and thermal (Saha-Boltzmann) number densities, respectively. The line list is extracted from Kurucz' (1994) compilation, and it includes all the atomic and molecular lines.

5. Results

5.1. NLTE effects

At T_{eff} and $\log g$ close to solar values the statistical equilibrium of Ba II is strongly affected by radiative processes in b-b transitions because this is the dominant ionization stage. As a consequence NLTE effects for Ba II depend on the Ba abundance which correlates with the general metallicity of the model atmosphere (see below). Thus, NLTE leads to a strengthening the Ba II lines compared with the LTE case at [M/H] > -2 and to the opposite effect at lower metallicities. We consider the mechanisms and the physics behind them for two extreme cases: a normal metallicity atmosphere and a metal-poor one. The Sun and G84-29 are taken as examples. In Fig. 2 the departure coefficients, b_i as a function of continuum optical depth τ_{5000} refering to $\lambda = 5000$ Åare shown for both stars. In the first place, we are interested in the behaviour of the levels necessary for subsequent line profile synthesis. These are $6s^2\mathrm{S}_{1/2}$, $6p^2\mathrm{P}^\circ_{1/2,3/2}$ and $5d^2\mathrm{D}_{3/2,5/2}$. In addition, we present the levels necessary for understanding the mechanisms of the continuum overpopulation displayed in Fig. 2.

In the solar atmosphere the ratio n(Ba II)/n(Ba III) exceeds 10 everywhere outside $\log \tau_{5000} = 0$ and becomes smaller only in the deeper layers. No process seems to affect the ground state population, and $6s$ keeps its thermodynamic value. The metastable level $5d$ follows the ground state due to collisional coupling, and only in the uppermost layers this coupling is lost. The departure coefficients of $6p^2\mathrm{P}^\circ_{1/2,3/2}$ begin to deviate from 1 at the depths around $\log \tau_{5000} = -2$ where photon losses in the weakest line λ585.3nm of the multiplet $5d$–$6p$ start to become important. The $6p$ underpopulation is amplified in the upper layers which are transparent with respect to the radiation of the two strong lines of that multiplet. It is interesting to note that NLTE effects on the $6s^2\mathrm{S}_{1/2}$, $6p^2\mathrm{P}^\circ_{1/2,3/2}$ and $5d^2\mathrm{D}_{3/2,5/2}$ level populations are caused by the transitions between the levels themselves. This confirms a common experience: three atomic levels are enough to produce departures from LTE. Thus, the Ba II term structure with the 3 lowest terms connected by two allowed transitions with energy separation of 1.9 and 2.6 eV is a prerequisite to NLTE effects in solar-like atmospheres where photons of a similar energy contain the larger part of a common flux. Nevertheless, to obtain accurate quantitative values of level populations we have to consider the upper Ba II levels, too.

An interesting result is the overpopulation of all the levels above $7s$ outside $\log \tau_{5000} = 0.4$ in solar atmosphere. This is

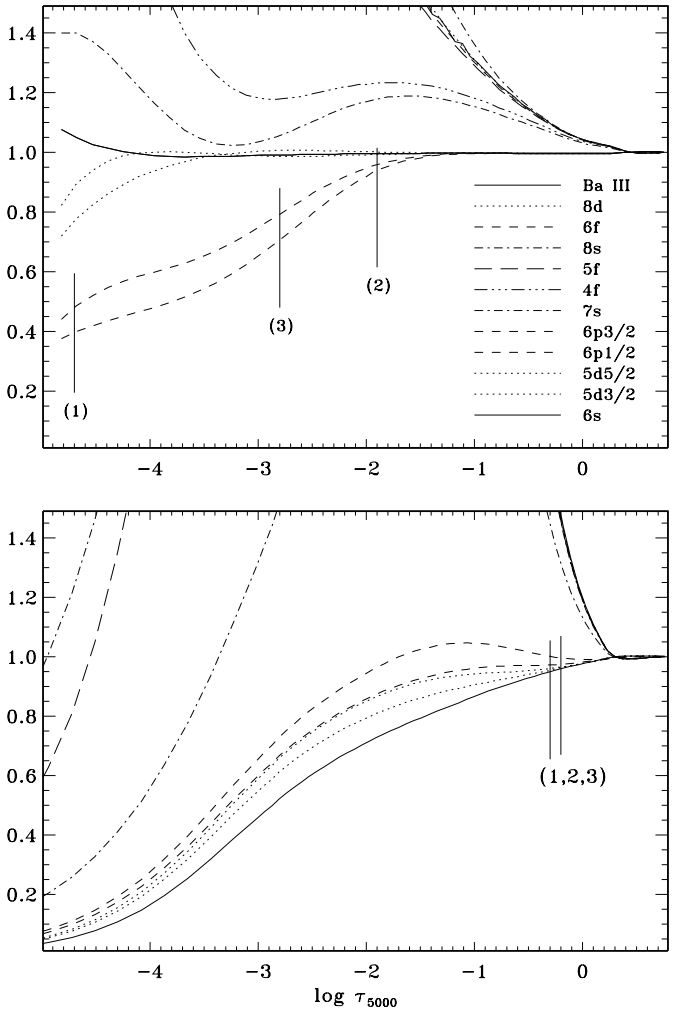

Fig. 2. Departure coefficients b_i for some levels of Ba II in the model atmospheres of the Sun (*top*) and G84-29 (*bottom*). Tick marks indicate the locations of line center optical depth unity for the Ba II lines λ455.4 nm (1), λ585.3 nm (2) and λ649.6 nm (3)

due to line pumping. Following Bruls et al. (1992) we use the term "pumping" for superthermal radiation of non-local origin producing enhanced excitation. Several transitions arising from $6p$ and $5d$ are pumped by $J_\nu - B_\nu(T_e)$ excess radiation in the layers where the line wing optical depth drops below 1. The $6p$–$7d$ transition with the multiplet lines around 263 nm and $6p$–$8s$ ($\sim$277 nm) turn to pumping outside $\log\tau_{5000}$ = 0.4. In even higher layers $6p$–$7s$ (413 nm), $6p$–$6d$ (490 nm), and then $5d$–$4f$ (232 nm) and $5d$–$5f$ (190 nm) are added. $5d$ and $6p$ are in thermal equilibrium with the ground state over the wide depth range; therefore the upper levels are overpopulated from the ground state electron reservoir. This is true for the continuum, too, because of its radiative and collisional coupling to the upper levels. From this behaviour of departure coefficients we expect that our Ba II lines of interest are amplified compared with the LTE case, because for each of them $b_u/b_l < 1$ is valid in line formation layers resulting in a source function S_{lu} smaller than $B_\nu(T_e)$.

In the metal-poor atmosphere of G84-29 the ionization equilibrium n(Ba II)/n(Ba III) is different from the solar ionization equilibrium because of smaller electron densities and slightly higher temperatures. Ba II dominates Ba III inside $\log\tau_{5000} = -3$, but everywhere n(Ba II)/n(Ba III) < 6. In the uppermost layers this ratio decreases to 0.01. The most striking and unexpected details found in Fig. 2b are the underpopulation of the Ba II ground state starting from the deep layers around $\log\tau_{5000} = 0$ and the depopulation of $5d$ and $6p$. This is the result of a number of processes. Let us consider line pumping first; this mechanism plays a more important role in a metal-poor atmosphere due to fewer collision processes. Outside $\log\tau_{5000}$ = 0 the resonance transition (λ455.4 nm) is pumped resulting in a depopulation of the ground state. The pumping transitions $6p$–$8s$, $-7d$, $-7s$, $-6d$ and especially $5d$–$4f$ depopulate $6p$ and $5d$ and favour the underpopulation of the ground state, too. Another mechanism is the overionization of $6p$. Due to less ultraviolet opacity in metal-poor atmospheres the radiation field near the threshold of $6p^2\mathrm{P}^\circ_{3/2}$ at 170.3 nm and $6p^2\mathrm{P}^\circ_{1/2}$ at 165.4 nm becomes superthermal far inside the atmosphere near $\log\tau_{5000} = -0.65$ and -0.87, respectively. As a result photoionization of these levels dominates depopulation processes leading to underpopulation of $6p$ and, consequently, the ground state. Finally, $5d$ sublevels are overpopulated relatively to the ground state by filling up from $6p$ sublevels via the line transitions in the layers transparent to the radiation of corresponding wavelengths, namely, at optical depths $\log\tau_{5000} \le -0.1$.

In contrast to the solar atmosphere Ba II lines in metal-poor atmospheres are weaker not only due to $b_u/b_l > 1$ (resulting in $S_{lu}/B_\nu(T_e) > 1$) but also by reducing the number density of the lower level, $b_l < 1$.

Consequently, similar mechanisms cause departures from LTE for the Ba II atom in atmospheres of normal metallicity and in metal-poor atmospheres. However, quantitative differences of physical parameters such as Ba abundance and electron number density lead to a different qualitative behaviour of departure coefficients, and they also cause opposite NLTE effects on the Ba II line intensities.

5.2. Solar Ba II lines

The Sun is chosen as the reference star with an observed spectrum of high quality and relatively well-known stellar parameters. These data are used to improve two kinds of atomic data important for subsequent analyses of the metal-poor stars. These are the efficiency of hydrogenic collisions in the Ba II statistical equilibrium and van der Waals damping constants, C_6.

We use solar flux observations taken from the Kitt Peak Solar Atlas (Kurucz et al. 1984). Our synthetic flux profiles are convolved with a profile that combines a rotational broadening of 1.8 km s^{-1} and broadening by macroturbulence with a radial-tangential profile of $V_{\rm mac} = 2.7$ km s^{-1}.

Assuming LTE we cannot fit solar Ba II line profiles with reasonable values of $\log\varepsilon_{\rm Ba}$ and $V_{\rm mic}$. NLTE profiles give a better though not excellent reproduction of the observations. The best fitting is presented in Fig. 3. For the solar Ba abun-

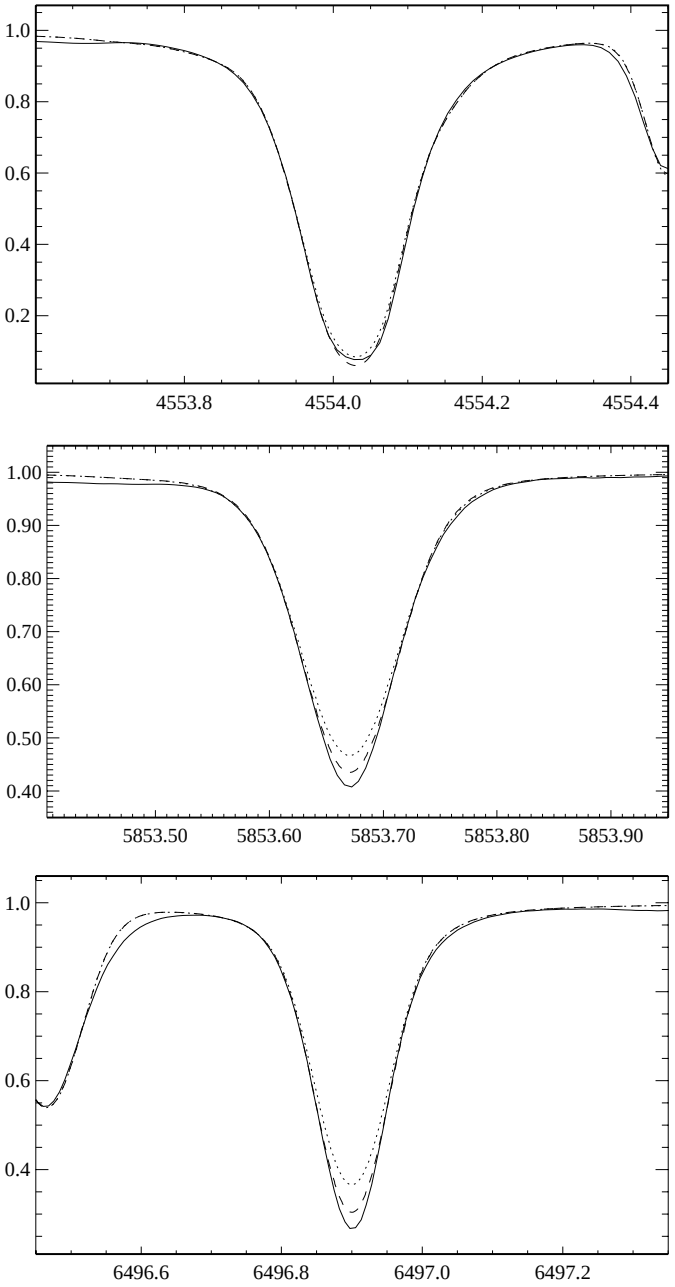

Fig. 3. Synthetic NLTE (dashed line) and LTE (dotted line) flux profiles of the Ba II lines compared with the observed spectrum of the Kurucz et al. (1984) solar flux atlas (continuous line). See text for discussion of the fitting parameters

dance we accept $\log \varepsilon_{\rm Ba,\odot} = 2.13$ from Anders& Grevesse (1989). A depth-independent microturbulence of 0.9 km s^{-1} is derived from λ455.4 nm and λ649.6 nm, and 0.85 km s^{-1} from λ585.3 nm. The corrections $\Delta \log C_6$ to the classic Unsöld (1955) collisional damping constant derived from solar line wing fitting are given in Table 2. For comparison the LTE profiles corresponding to the same fitting parameters are presented in Fig. 3, too.

It can be seen from Fig. 3 that NLTE effects are important for the subordinate lines. The NLTE line core of λ649.6 nm is deeper by 6.5% of the continuum flux than the LTE one. The discrepancies between the NLTE and LTE profiles can be seen in the region of the shoulder between core and wing up to relative intensities of about 0.8. It means that even C_6 cannot be derived reliably assuming LTE.

The NLTE resonance line core is deeper than observed one by only 1.5% of the continuum flux. It is formed in the uppermost atmospheric layers near $\log \tau_{5000} = -4.7$ (cf. Fig. 2), and it is most probably influenced by a non-thermal and depth-dependent chromospheric velocity field that is not part of our solar model (the chromospheric temperature rise is expected to be less important because Ba II is the dominant ionization stage). For this reason we are not able to fit the observed λ455.4 nm line core and we are forced to use a slightly larger value of $V_{\rm mac} = 2.8$ km s^{-1} to describe the halfwidth of this line compared with the 2.7 km s^{-1} required to adjust the subordinate lines. An even stronger chromospheric effect on λ455.4 nm has been found for Procyon. Only taking $V_{\rm mic}$ = 2.1 km s^{-1} and $V_{\rm mac}$ = 7.5 km s^{-1} we can fit the Ba II resonance line in the Procyon spectrum where $V_{\rm mic}$ = 1.9 km s^{-1} and $V_{\rm mac}$ = 6.3 km s^{-1} are needed to adjust the subordinate lines. The chromospheric influence is expected to be negligible for metal-poor stars because resonance line formation is shifted to deeper layers. In fact we have not found any discrepancies of fitting parameters between λ455.4 nm and the subordinate lines in subsequent analyses of the metal-poor stars.

Let us go back to the subordinate lines λ585.3 nm and λ649.6 nm. Fig. 3 shows that their theoretical line cores are too shallow compared with the observations. A number of test runs with different adjustments to the atomic model has been performed to investigate these discrepancies. We tested the influence of those atomic parameters which are not so well known. First of all, we compared different atomic models excluding and including H atom collisions with cross-sections calculated according to Steenbock & Holweger (1984) and scaled by various factors $k_{\rm H}$. The inclusion of H atom collisions has no effect on the resonance line, but it makes the NLTE profiles of the subordinate lines more shallow by 1.5% of the continuum flux for λ585.3 nm and by 4% for λ649.6 nm, with $k_{\rm H}$ increasing from 0 to 1. The NLTE profiles in Fig. 3 correspond to $k_{\rm H}$ = 1/3. Excluding H atom collisions ($k_{\rm H}$ = 0) makes the profiles deeper by only 2% for λ649.6 nm and 0.8% for λ585.3 nm. This is again not sufficient to fit the solar profiles. Next, electronic collision cross-sections were scaled for individual transitions such as the important transition $6s$–$5d$ (10 times) and the fine structure transitions between $5d$ sublevels and $6p$ sublevels (10 times) and also for all the forbidden transitions (1000 times). In addition, photoionization cross-sections were scaled by a factor 10 (both increased and decreased) for the important levels $8s$, $7d$ and $6p$. In total, we were able to increase the line center depth of the subordinate line profiles by only 1% of continuum flux while no change was calculated for the resonance line center. This confirms once more that for solar type stars departures from LTE for the Ba II atom are mainly due to radiative b-b transitions. Their atomic parameters are well known, so, NLTE effects turn out to be fixed, and we are not able to explain the

differences between the observed and theoretical line profiles by uncertainties of the NLTE calculations. We suggest that the observed Ba II profiles reflect a more realistic depth-dependent velocity field which can be described by hydrodynamical models of the solar atmosphere. Due to high sensitivity to motions of emitting matter the Ba II lines can be recommended to test such models. Though for last decade the hydrodynamical models of solar atmosphere have being in progress they are still not sufficient to fit solar profiles. And we are forced to use one-dimensional homogenious model atmospheres to extract useful information from the solar spectrum.

Our test calculations show that we are not able to estimate the efficiency of hydrogenic collisions only from solar Ba II lines because of the small effect on the theoretical profiles for solar parameters. However, we find it from analyses of the metal-poor stars where hydrogenic collisions are more important. Below we give proof that the scaling factor $k_{\rm H}$ = 1/3 is appropriate.

5.3. Barium abundances for the stars

Only the Ba II resonance line λ455.4 nm occurs in spectra of all the stars of our sample. The subordinate lines λ649.6 nm and λ585.3 nm disappear at [Fe/H]< -2.3 and < -1.9, respectively. In addition λ649.6 nm was not used in the analyses of HD19445 and HD140283 because of its superposition with telluric lines.

Ba abundances are determined from line profile fitting and we first need to know the rotational velocity $V \sin i$ and macroturbulence value $V_{\rm mac}$. All the stars of our sample are slow rotators. Therefore the instrumental profile (a Gaussian of 4.6 km s^{-1} for the September 1995 spectra and 3.2 km s^{-1} for the May 1997 spectra) acts as the dominant contributor to the convolution profile. $V \sin i$ and $V_{\rm mac}$ cannot be separated at the spectral resolving power we have, and we treat their total action as radial-tangential macroturbulence. With the known instrumental profile $V_{\rm mac}$ is deduced from the observed line shape. The values of $V_{\rm mac}$ from different Ba II lines are very close together for each of the stars except for Procyon and HD 45282 which require a greater $V_{\rm mac}$ for the resonance line. Procyon is the hottest star of our selection with maximum microturbulence ($V_{\rm mic} = 1.9$ km s^{-1} from subordinate lines) and maximum macroturbulence ($V_{\rm mac} = 6.3$ km s^{-1} from subordinate lines), and most probably with important chromospheric contributions. As discussed above the λ455.4 nm line core is evidently affected by the chromospheric velocity field. HD 45282 is the most luminous star of our sample with the most extended atmosphere. Although it is a metal-poor star the λ455.4 nm line core is formed in upper atmospheric layers at $\log \tau_{5000} = -3.6$. $V_{\rm mac} = 5.3$ km s^{-1} from the resonance line (as compared with $V_{\rm mac} = 2.8$ km s^{-1} from the subordinate lines) most probably reflects chromospheric influence, too. In Fig. 4 we show as an example the Ba II line profile fitting for two stars of our sample, HD 45282 and HD 103095.

For three metal-poor stars observed in September 1995, HD 6582, HD 194598 and HD 201891 the weakest Ba II line λ585.3 nm shows a triangular shape due to insufficient spectral resolving power. In these cases the observed equivalent widths are used to estimate Ba abundance. Fortunately, at those stellar parameters λ585.3 nm is weak enough and its W_λ is nearly insensitive to $V_{\rm mic}$ and collisional damping.

As mentioned above two lines of the same multiplet λ585.3 nm and λ649.6 nm show different NLTE effects. We have used this fact to derive the influence of hydrogenic collisions on the statistical equilibrium of Ba II. For 6 stars with both lines observed we have considered NLTE abundance corrections $\Delta_{\rm NLTE} = \log \varepsilon_{\rm LTE} - \log \varepsilon_{\rm NLTE}$. HD 103095 has been excluded because of negligible NLTE effects in both lines. For λ585.3 nm $\Delta_{\rm NLTE}$ does not exceed 0.07 dex, and it drops to only 0.01 dex for the metal-poor stars. Therefore, Ba abundances from λ585.3 nm depend only slightly on the scaling factor $k_{\rm H}$, whereas values for $\Delta_{\rm NLTE}$ obtained from λ649.6 nm range from 0.2 dex (Procyon) down to 0.08 dex (HD 194598) and are affected by $k_{\rm H}$. The value of $k_{\rm H}$ can thus be found from the requirement that Ba abundances derived from both lines must be equal. The differences $\log \varepsilon(\lambda 649.6\,{\rm nm}) - \log \varepsilon(\lambda 585.3\,{\rm nm})$ averaged over 6 stars are 0.07 dex with respect to the LTE assumption, -0.04 dex for $k_{\rm H}$ = 0 and -0.01 dex for $k_{\rm H}$ = 1/3. It can be seen that NLTE effects are overestimated for λ649.6 nm if hydrogenic collisions are neglected. $k_{\rm H}$ = 1/3 is appropriate and this value is adopted in our study.

In Table 4 we give NLTE and LTE barium abundances from three Ba II lines. The typical discrepancy between NLTE abundances from various lines is 0.02 dex and only for HD 45282 it reaches 0.06 dex. [Ba/Fe] ratios are plotted as function of metallicity, and the results both for NLTE and LTE cases are presented

Table 4. Stellar Ba abundances

Object/HD	[Fe/H]		[Ba/H]		
			λ455.4	λ585.3	λ649.6
Procyon	0.0	NLTE		−0.02	−0.02
		LTE		0.03	0.15
HD6582	−0.83	NLTE	−0.81	−0.83	−0.83
		LTE	-0.78	−0.81	−0.76
HD19445	−1.97	NLTE	−2.00		
		LTE	−2.03		
HD45282	−1.50	NLTE	−1.39	−1.41	−1.45
		LTE	−1.32	−1.41	−1.33
HD103095	−1.36	NLTE	−1.26	−1.27	−1.26
		LTE	−1.24	−1.27	−1.24
HD140283	−2.30	NLTE	−2.95		
		LTE	−3.10		
HD186408	0.05	NLTE	0.10	0.09	0.09
		LTE	0.12	0.14	0.19
HD194598	−1.21	NLTE	−1.10	−1.12	−1.13
		LTE	−1.05	−1.12	−1.08
HD201891	−1.05	NLTE	−1.00	−1.03	−1.03
		LTE	−0.95	−1.03	−0.95
G246-38	−2.20	NLTE	−2.04		−2.04
		LTE	−2.04		−2.05
G84-29	−2.60	NLTE	−3.07		
		LTE	−3.27		

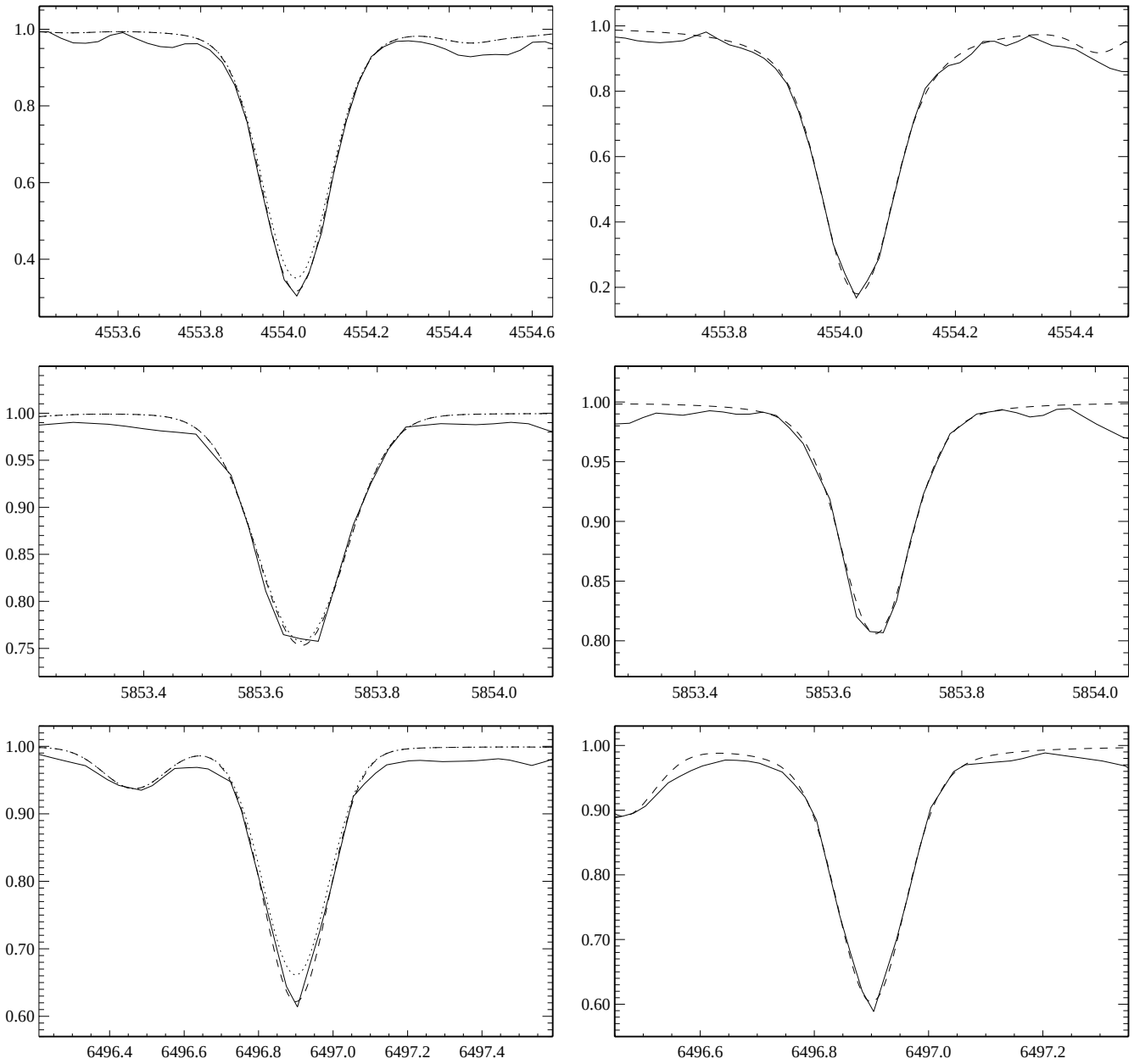

Fig. 4. Synthetic NLTE (dashed line) and LTE (dotted line) flux profiles of Ba II lines compared with the observed FOCES spectra (continuous line) of HD 45282 ($\lambda/\Delta\lambda = 40000$) (*left column*) and HD 103095 ($\lambda/\Delta\lambda = 60000$) (*right column*). For HD 103095 only the NLTE profiles are shown because the NLTE effects are small

in Fig. 5. It can be seen that at [Fe/H] ≥ -2.2 there is no trend of [Ba/Fe] with [Fe/H] and Ba to Fe abundance ratios are actually solar. For two stars with [Fe/H] = -2.3 and -2.6 barium is underabundant relative to iron. Only the resonance line is observed for both stars and it is very weak. The spectral resolving power of 40000 turns out not to be sufficient to produce a λ455.4 nm line profile. We estimate the uncertainty of Ba abundances for HD 140283 and G84-29 as ± 0.1 dex. To make sure that the Ba underabundance is reliable we have determined for both stars the abundance of another neutron capture element, strontium. We use the Sr II resonance line λ421.5 nm which is free of blends in spectra of extremely metal-poor stars. This line is stronger than the Ba II resonance line and for both stars its observed profile is well fitted by theoretical one. The theoretical NLTE line profiles are obtained with 41-level model atom of Sr II described in Belyakova & Mashonkina (1997). [Sr/H] is found as -2.82 and -3.07 for HD 140283 and G84-29 correspondingly. This means that Sr is also underabundant in atmospheres of these stars and the magnitudes of the Sr and Ba deficiency are close: [Sr/Fe] = -0.52 dex and [Ba/Fe] = -0.65 dex for HD 140283, and the same value of -0.47 dex is obtained for [Sr/Fe] and [Ba/Fe] in the case of G84-29. These results confirm the superdeficiency of heavy elements synthesized through neutron capture reactions in atmospheres of very metal-poor stars found by other

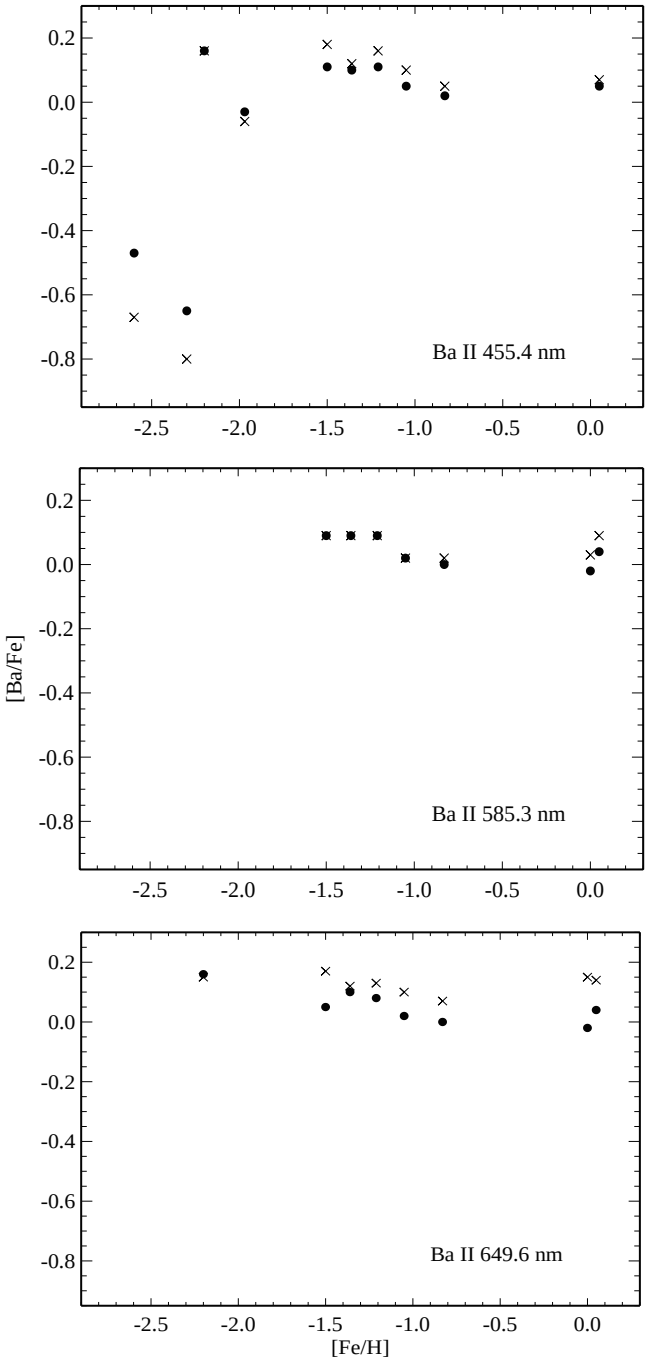

Fig. 5. The run of [Ba/Fe] with [Fe/H] for three Ba II lines. Symbols correspond to NLTE (filled circles) and LTE (crosses) barium abundances

authors (Mathews et al. 1992; Ryan et al. 1990 and references therein). However we find the run of [Ba/Fe] with [Fe/H] is non-monotonic and there is the jump of Ba abundances of about 0.5 dex at metallicity between -2.2 and -2.3.

Summing up the above results of our NLTE analysis we conclude that Ba follows the Fe production in a phase of Galactic evolution starting at [Fe/H] ~ -2.2. In the even more metal-poor stars Ba is underabundant relative to iron changing with a step of 0.5 dex. On one hand, our results are in qualitative agreement with the theoretical models of the s-process which predict the depletion of barium in the oldest stars (Mathews et al. 1992), but on the other hand, a step-like change of the Ba abundance at [Fe/H] ~ -2.3 and similar rates of Ba and Fe production in the later phases of the Galaxy evolution still await explanation by theory.

5.4. The r/s-process controversy

Truran (1981) has suggested that the r-process dominated the production of heavy elements in very metal-poor stars. Some abundance studies of halo stars gave arguments for this hypothesis. Sneden & Parthasarathy (1983) and Gilroy et al. (1988) found the heavy element abundance patterns consistent with nucleosynthesis dominated by the r-process. On the other hand, Gratton & Sneden (1994) concluded that the abundance patterns of neutron-capture elements in metal-poor stars show clear differences with respect to the scaled solar system r-process nucleosynthesis predictions. Magain (1995) has reviewed and rediscussed spectroscopic data (Sneden & Parthasarathy 1983; Gilroy et al. 1988; Gratton & Sneden 1994), and he has shown that no reliable observational evidence is found in support of Truran's hypothesis. Magain has first determined the relative importance of the s- and r-process in Ba production for the metal-poor star HD 140283. As mentioned above the even Ba isotopes are mostly produced by the s-process while the r-process contribution dominates the odd isotopes and the odd-to-even isotopic ratio is thus a measure of the r- to s-process ratio. The resonance line of the odd isotopes has several HFS components and this leads to an additional broadening of the line. Magain used the fact that a larger r-process contribution implies a larger fraction of odd isotopes and, consequently, a broader spectral line. Using a spectrograph with a resolving power of 100000 he has measured the broadening of the λ455.4 nm line profile for HD 140283 deriving an isotopic ratio very close to solar. It means that in the interstellar matter out of which this star formed the total contribution of the s-process to Ba production dominated the r-process. Later, the abundance pattern for elements heavier than Ba was found to be identical to the solar system r-process pattern in the star CS 22892-052 (Sneden et al. 1996). Another star, the metal-poor halo giant, HD126238 ([Fe/H] = -1.7) shows a heavy element pattern containing 80% r-process and 20% solar system mixture (Cowan et al. 1996). So, the problem of whether nucleosynthesis of the heavy elements occurred by the s-process or r-process has not yet been solved, and it would be useful to estimate the s- to r-process relation for a larger sample of stars.

In this paper we present a direct method of determining the odd-to-even isotopic ratio from the Ba II resonance line provided that the Ba total abundance is determined from subordinate Ba II lines free of HFS splitting. The relative strengths of the λ455.4 nm HFS components depend on the odd-to-even isotopic ratio. The pure r-process produces mainly the odd isotopes ^{135}Ba and ^{137}Ba resulting in only two HFS components with f_{ij} given in Table 5. The pure s-process produces the even

Table 5. Oscillator strengths of the HFS components for different Ba isotopic ratios

λ [nm]	isotopes included	solar mixture	s-process	r-process
455.4034	^{138}Ba + ^{136}Ba	0.597	0.666	–
455.4052	^{135}Ba + ^{137}Ba	0.081	0.038	0.454
455.4000	^{135}Ba + ^{137}Ba	0.049	0.023	0.273

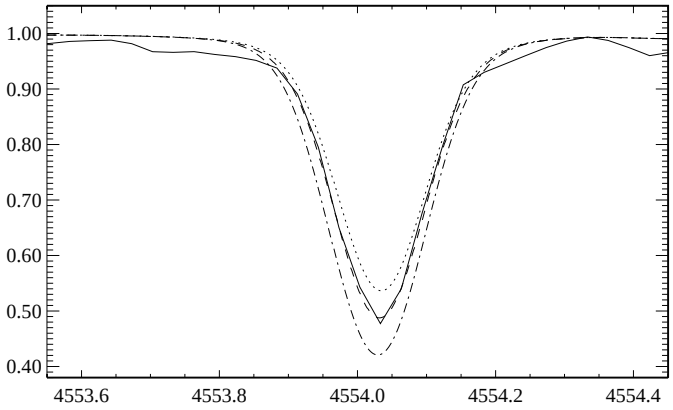

Fig. 6. Synthetic NLTE flux profiles of the Ba II resonance line compared with the observed FOCES spectrum of G246-38 (continuous line). The different lines correspond to different models of Ba synthesis: solar ratio of the s- to r-process (dashed line); pure s-process (dotted line) and pure r-process (dot-dashed line). The same value of the Ba abundance [Ba/H] = −2.04 obtained from λ649.6 nm is adopted in these computations

isotopes and ^{137}Ba resulting in three components. Their f_{ij} have been estimated from the assumption that n(^{137}Ba)/n(*even isotopes*) is 0.09 which is the solar ratio of the fraction of ^{137}Ba produced by the s-process to the fraction of even isotopes. Our method is based on the fact that the larger the r-process contribution is the larger the fraction of odd isotopes must be, and the greater the total energy absorbed in the resonance line whereas the subordinate lines remain unchanged. This provides an important advantage of our method which does not require an extremely high spectral resolving power because we need only measure the total energy absorbed in the spectral line (i.e. its equivalent width) and not examine line broadening and resolved profiles.

For the very metal-poor star G246-38 with both resonance and subordinate lines observed we have established the Ba abundance from λ649.6 nm; then the λ455.4 nm line profiles were calculated with the same $\log \varepsilon_{\rm Ba}$ for three models of Ba synthesis: a pure r-process, a pure s-process, and a solar ratio of the s- to r-process contributions. In Fig. 6 they are superposed on the observed profile. The best fit is evidently obtained for a solar mixture of Ba isotopes. For the pure r-process the theoretical profile is deeper than the observed one and to agree with observations the Ba abundance would have to be reduced by 0.2 dex. This is a rather large value and we do not expect that the Ba abundance determined from λ649.6 nm is wrong by that amount. Therefore we conclude that both the Sun and the star with [Fe/H] = −2.2 have been formed from matter with barium produced mainly by the s-process. The similar calculations for HD 45282 show even greater divergence between Ba abundances from the subordinate lines and from λ455.4 nm if a pure r-process is suggested. It amounts to 0.3 dex while a solar mixture of Ba isotopes provides a good agreement between theoretical and observed profiles. These results are direct and precise determinations of Ba isotopic ratios for two metal-poor stars. Unfortunately, we are not able to perform similar analyses for the most metal-poor stars of our sample because λ649.6 nm is blended by the telluric lines for HD 140283 and it cannot be extracted from noise for G84-29.

As a result we do not find observational arguments for the hypothesis that the r-process dominated Ba production at early phases of the Galactic evolution. We emphasize that the estimated relative importance of the s- and r-process together with the improved [Ba/Fe]–[Fe/H] dependence will serve as significant observational constraints to theoretical models of the chemical evolution of the Galaxy.

Acknowledgements. ML thanks the Institute of Astronomy and Astrophysics of Munich University for warm hospitality during a productive stay in September–December 1997 and the "Deutscher Akademischer Austauschdienst" for the partial support of this study. The authors thank K. Fuhrmann for providing the reduced FOCES spectra of most of the stars investigated in this paper, for valuable help and many useful discussions. F.Grupp is thanked for providing the reduced FOCES spectrum of G246-38. We are grateful to H.Karlsson and J.Pickering for sending us the references on HFS in Ba II. ML and BI have been partially supported also by the Russian Basic Researches Fund (grant 96-02-16306-a).

References

Allen C.W., 1973, Astrophysical Quantities. Athlone Press
Anders E., Grevesse N., 1989, Geoch. & Cosmochim Acta 53, 197
Auer L.H., Heasley J., 1976, ApJ 205, 165
Becker W., Werth G., 1983, Z.Phys. A311, 41
Belyakova E.V., Mashonkina L.I., 1997, Astron.Rep. 41, 109
Bergbusch P.A., VandenBerg D.A., 1992, ApJS 81, 163
Biehl D., 1976, Sonderdruck der Sternwarte Kiel, No.229
Bikmaev I.F., Mashonkina L.I., Sakhibullin N.A., Shimanskaya N.N., Shimansky V.V., 1996, Chemical and Dynamical History of the Milky Way. In: Blitz L., Teuben P. (eds.) Proc.IAU Symp. 169, Unsolved Problems of the Milky Way. Reidel, Dordrecht, p. 389
Blatt R., Werth G., 1982, Phys. Rev A25, 1476
Brix F., Kopfermann H., 1952, Landolt-Börnstein, I/5, Springer, Berlin
Bruls J.H., Rutten R.J., Shchukina N., 1992, A&A 265, 237
Burris D.L., Pilachowski C.A., Armandroff T., Cowan J.J., Sneden C., 1998, in preparation
Cameron A.G.W., 1982, Ap&SS 82, 123
Cowan J.J., Sneden C., Truran J.W., Burris D.L. 1996, ApJ 460, L115
Cowley C.R., Frey M., 1989, ApJ 346, 1030
Crandall D.H., Taylor P.O., Dunn G.H., 1974, Phys. Rev. A10, 141
Doyle R.O., 1968, ApJ 153, 987
Drawin H.-W., 1961, Z.Physik 164, 513
Drawin H.-W., 1968, Z.Physik 211, 404
Edvardsson B., Andersen J., Gustafsson B., et al., 1993, A&A 275, 101

ESA 1997, The Hipparcos and Tycho Catalogues. ESA SP-1200
Feeney R.K., Hooper J.W., Elford M.T., 1972, Phys.Rev. A6, 1469
Fleurier C., Sahal-Brechot S., Chapelle J., 1977, JQSRT 17, 595
Fuhrmann K., Axer M., Gehren T., 1993, A&A 271, 451
Fuhrmann K., Pfeiffer M., Frank C., Reetz J., Gehren T., 1997a, A&A 323, 909
Fuhrmann K., Pfeiffer M.J., Bernkopf J., 1997b, A&A 326, 1081 0
Fuhrmann K., 1998, A&A, in press
Gilroy K.K., Sneden C., Pilachowski C.A., Cowan J.J., 1988, ApJ 327, 298
Gratton R.G., Sneden C., 1994, A&A 287, 927
Gray D.F., 1977, ApJ 218, 530
Grupp F., 1997, Diploma Thesis, Universität München
Hofsaess D., 1979, Atomic Data and Nuclear Data Tables 24, 285 (and private communication)
Holweger H., 1979, In: Les Elements et leurs Isotopes dans l'Univers. 22nd Liège Symp., Liège, p. 117
Holweger H., Müller E., 1974, Solar Phys. 39, 19
Kurucz R.L., 1994, CD-ROM 18
Kurucz R.L., Furenlid I., Brault J., Testerman L., 1984, Solar Flux Atlas from 296 to 1300 nm. Nat. Solar Obs., Sunspot, New Mexico
Leep E.M., Wallerstein G., 1981, MNRAS 196, 543
Lindgard A., Nielsen S.E., 1977, Atomic Data Nucl. Data Tables 19, 533
Magain P., 1989, A&A 209, 211
Magain P., 1995, A&A 297, 686
Magain P., Zhao G., 1993, A&A 268, L27
Mashonkina L.I., Bikmaev I.F., 1996, Astron.Rep. 40, 109
Mathews G.J., Bazan G., Cowan J.J., 1992, ApJ 391, 719
Miles B.M., Wiese W.L., 1969, Atomic Data 1, 1
Nissen P.E., Hog E., Schuster W.J., 1997, Surface Gravities of Metal-poor Stars Derived from Hipparcos Parallaxes. In: Proc. HIPPARCOS Venice Symp. ESA SP-402
Peart B., Stevenson J.G., Dolder K.T., 1973, J.Phys. B6, 146
Peterson R.C., Kurucz R.L., Carney B.W.. 1990, ApJ 350, 173
Pfeiffer M., Frank C., Baumüller D., Fuhrmann K., Gehren T., 1998, A&AS 130, 381
Platisa M., Puric J., Konjevic N., Labat J., 1971, A&A 15, 325
Roig R.A., Tondello G., 1975, J.Opt.Soc.America 65, 829
Rutten R.J., 1978, Solar Phys. 56, 237
Ryan S.G., Norris J.E., Beers T.C., 1996, ApJ 471, 254
Sakhibullin N.A., 1983, Trudi Kazan gor.obs. 48, 9
Shevelko V.P., 1974, Optics Spectrosc. 36, 7
Silverans R.E., Borghs G., Dumont G., Van den Cruyce J.M., 1980, Z.Phys. A295, 311
Sobelman I.I., Vainshtein L.A., Yukov E.A., 1981, Excitation of Atoms and Broadening of Spectral Lines. Springer Series Chem. Phys. 7. Springer, Berlin, Heidelberg, New York
Sneden C., McWilliam A., Preston G.W., et al., 1996, ApJ 467, 819
Sneden C., Parthasarathy M., 1983, ApJ 267, 757
Spite M., Spite F., 1979, A&A 76, 150
Steenbock W., Holweger H., 1984, A&A 130, 319
Takeda Y., 1992, A&A 242, 455
Truran J.W., 1981, A&A 97, 391
Unsöld A., 1955, Physik der Sternatmosphären. 2nd edition, Springer, Berlin - Göttingen - Heidelberg
VandenBerg D.A., 1992, ApJ 391, 685
van Regemorter H., 1962, ApJ 136, 906
Wiese W.L., Martin G.A., 1980, Wavelengths and Transition. Probabilities for Atoms and Atomic Ions. Part II. NSRDS - NBS 68, Washington, D.C.